Article

UDC 548.73:539.23:621.3.049:620.9
https://doi.org/10.31489/2026PH1/69-80

Received: 23.10.2025
Accepted: 01.12.2025

Sh. Afroze[1, 2, 3], A.M. Kabyshev[1]✉, A.A. Aimakhanova[1],
M.S. Reza[2], M.S. Islam[4], K.A. Kuterbekov[1], A.K. Azad[2]

[1]*Institute of Physical and Technical Sciences, L.N. Gumilyov Eurasian National University, Astana, Kazakhstan;*
[2]*University Brunei Darussalam, Bandar Seri Begawan, Brunei;*
[3]*Chalmers University of Technology, Gothenburg, Sweden;*
[4]*Bangladesh University of Engineering and Technology, Dhaka, Bangladesh*

A Study of Structural and Thermal Properties of a Novel Doped Perovskite-Type Oxide $SrFe_{0.6}Cu_{0.3}Mo_{0.1}O_{3-\delta}$

In this study, a novel perovskite-type oxide $SrFe_{0.6}Cu_{0.3}Mo_{0.1}O_{3-\delta}$ was synthesized via a conventional solid-state reaction route and comprehensively characterized using neutron powder diffraction (NPD), scanning electron microscopy (SEM), and thermal analysis. The application of NPD enabled precise determination of the atomic structure and differentiation between cations with similar atomic numbers. Rietveld refinement of the NPD data confirmed the formation of a single-phase cubic perovskite with the space group *Pm*-3*m* (no. 221) and a lattice parameter of $a = b = c = 3.8997(1)$ Å. SEM images revealed a highly porous, interconnected microstructure with uniform elemental distribution, while thermogravimetric analysis (TGA) demonstrated a two-step oxygen loss up to 1000 °C, confirming excellent thermal stability. The oxide exhibited a low thermal conductivity of 1.986 $W \cdot m^{-1} \cdot K^{-1}$ at 900 °C, attributed to enhanced phonon scattering induced by Cu and Mo co-doping and lattice disorder. These findings indicate that controlled B-site co-doping can effectively tailor defect chemistry and phonon transport, resulting in materials with reduced thermal conductivity and improved structural integrity. Therefore, $SrFe_{0.6}Cu_{0.3}Mo_{0.1}O_{3-\delta}$ shows great potential for high-temperature energy conversion applications, including thermoelectric devices and solid oxide fuel cells.

Keywords: perovskite oxide, neutron powder diffraction, Rietveld refinement, solid-state synthesis, scanning electron microscopy, thermogravimetric analysis, microstructure, oxygen non-stoichiometry, phonon scattering, thermal conductivity

✉*Corresponding author*: Kabyshev, Asset, kabyshev_am_1@enu.kz

Introduction

Perovskite-type oxides (ABX_3) were first identified in the mineral $CaTiO_3$, where A and B are cations and X is an anion. The perovskite lattice exhibits remarkable compositional flexibility, nearly all transition metals, lanthanides, and actinides can occupy the B-site, while larger alkali, alkaline-earth, or rare-earth ions occupy the A-site with twelve-fold oxygen coordination [1]. Doped perovskites with general formulas $A^{2+}B^{4+}O_3$, $A^{1+}B^{5+}O_3$, or $A^{3+}B^{3+}O_3$ have been widely studied because of their tunable physical and chemical properties [2]. Achieving single-phase perovskite oxides often requires high calcination temperatures and long sintering durations, especially when refractory metal oxides are incorporated [3–5]. Consequently, these materials have found broad applications in energy conversion and storage, superconductivity, ferroelectrics, piezoelectrics, and electrodes, owing to their excellent electrical, magnetic, and pyroelectric properties [6–18].

Neutron powder diffraction (NPD) provides a powerful tool for elucidating the atomic structures of such materials. Unlike X-ray diffraction, neutron scattering lengths are largely independent of atomic number, allowing accurate localization of light atoms (e.g., H, Li, O) and differentiation between neighboring elements or isotopes [19, 20]. As a result, NPD has become increasingly important for investigating advanced energy materials [21–23].

In thermoelectric and solid-oxide fuel cell (SOFC) applications, low thermal conductivity is desirable to minimize heat loss and enhance efficiency. While pristine $SrTiO_3$ exhibits relatively high thermal conductivity, targeted doping at the Sr- or Ti-site can effectively suppress phonon transport [24–29]. For example, La^{3+}, Sm^{3+}, and Y^{3+} substitutions at the Sr-site, or Nb-doping at the Ti-site, have yielded significant reductions in thermal conductivity.

Building upon this concept, we developed a co-doped perovskite $SrFe_{0.6}Cu_{0.3}Mo_{0.1}O_{3-\delta}$, introducing Cu and Mo at the B-site to tailor the crystal structure and defect chemistry. Using high-resolution time-of-flight neutron diffraction, we accurately determined the crystal symmetry and atomic arrangement, confirming a cubic perovskite phase with space group *Pm*-3*m*. Additionally, we investigated its microstructural morphology and thermal transport behavior to elucidate the structure–property relationship. The findings demonstrate that controlled B-site co-doping can effectively lower thermal conductivity without compromising structural stability, suggesting potential use in high-temperature electrochemical and thermoelectric systems [30].

Materials and methods

Grinding the powder particles mostly with mortar and pestle to homogenize the combination of reactants is referred to in solid-state synthesis [31–35]. Repeated grinding and firing of the compound until it achieves a single phase is used in this method. Polycrystalline sample of the $SrFe_{0.6}Cu_{0.3}Mo_{0.1}O_{3-\delta}$ was synthesized through a solid-state route by using $SrCO_3$ (≥99.90 %, Aldrich), Fe_2O_3 (≥99.998 %, Aldrich), CuO, and MoO_3 (≥99.50 %, Aldrich) ceramic powders with the inclusion of ethanol as a dispersing agent, the powders were manually ground in an agate mortar by a pestle. The hydraulic press was employed to pelletize the mixed powders, placed in α-Al_2O_3 crucibles, and annealed at elevated temperatures in a box furnace. The mixture of the powder samples was first annealed at 650 °C for 10 hours. After pelletizing, annealed at 900 °C for 12 hours, then sintered at 1100 °C for 12 hours, with intermediate grinding and pelletizing. The entire synthesis process was carried out in air.

Prior to neutron powder diffraction, XRD was used to determine the phase structure using a Bruker axs-D8 Advance diffractometer. At the ISIS Neutron & Muon Source in the UK, neutron powder diffraction data were acquired using the Polaris diffractometer (medium-resolution powder diffractometer at a high intensity) [36, 37]. Utilizing GSAS-II software [38], the time-of-flight (TOF) powder diffraction data were analyzed. Standard parameters were used in the Rietveld analysis to refine the results, including a shifted Chebyshev series as background that was initiated by the GSAS software, zero shift, scale factor, profile parameters (type 3 in GSAS), cell parameters, atomic coordinates, site-occupancy factor (SOF), and atomic displacement factors (ADP).

Scanning electron microscopy (SEM) was used to examine the morphological structure and to evaluate its porosity. Since the sample was extremely conductive, a coating of carbon was applied to prevent overcharging. The JSM-7610F (Japan Electron Optics Laboratory Co. Ltd., Japan) was used to capture the pictures of the surface of the pellet, and it gave an outstanding, high-contrast view of the pellet. Netzsch-Gerätebau GmbH-STA 409 PC Luxx Simultaneous Thermal Analyzer was employed to perform TGA in order to observe the weight change with rising temperature under flowing N_2. $SrFe_{0.6}Cu_{0.3}Mo_{0.1}O_{3-\delta}$ powder weighing 68.342 mg was put in an Al_2O_3 DSC/TG pan and heated at a rate of 5 °C/min while flowing N_2 at a rate of 20 ml/min. Before cooling, an hour of isothermal holding eliminated the absorbed species. To confirm that all pollutants had completely been desorbed, the procedure was then repeated. Once the desorption process was finished, N_2 flow was used in place of airflow, and the mass change was monitored until equilibrium was attained. A Netzsch-DSC 4044F1 was employed to perform differential scanning calorimetry in order to observe the heat flow with rising temperature under a flowing inert atmosphere (Ar). A Netzsch-LFA 467 HT/Hyper Flash was used to determine the thermal conductivity at a rate of 5 °C/min while flowing Ar at a rate of 20 ml/min.

Results and discussion

Crystal Structure Analysis

Perovskite oxides offer remarkable compositional flexibility due to the wide range of possible substitutions at both the A and B sites, enabling precise control over oxygen vacancy concentration, redox-active centers, and physicochemical properties [39, 40]. Fe-doped $SrTiO_3$ compositions such as $SrTi_{0.3}Fe_{0.7}O_{3-\delta}$ and $SrTi_{0.6}Fe_{0.4}O_{3-\delta}$ have demonstrated excellent anode performance for solid oxide fuel cells (SOFCs) when combined with $Ce_{0.9}Gd_{0.1}O_{2-\delta}$, as reported by Sungmee et al. [41].

In this study, the X-ray diffraction pattern of $SrFe_{0.6}Cu_{0.3}Mo_{0.1}O_{3-\delta}$ synthesized via the solid-state route revealed a single-phase cubic perovskite structure with space group *Pm*-3*m* (no. 221). To achieve a deeper understanding of its crystal structure, neutron powder diffraction (NPD) measurements were carried out at room temperature (Fig. 1). Rietveld refinement of the NPD data confirmed the single-phase cubic symmetry, with refined lattice parameters of $a = b = c = 3.8997(1)$ Å, consistent with the simple perovskite framework (*a*□×*a*□×*a*□) where a□ is the primitive perovskite lattice parameter [42].

The diffraction data were refined using Bank 2 (up to 7 Å) of the POLARIS diffractometer. The refinement statistics and structural parameters are summarized in Table 1. The obtained low *R*-factors (*R*□ = 2.94 %, R_{wp} = 4.36 %, and R_f = 3.38 %) indicate excellent agreement between the observed and calculated profiles. The refined atomic positions, isotropic displacement parameters (U_{iso}), and Wyckoff sites confirm a well-ordered cubic structure without secondary phases or superstructure reflections associated with oxygen vacancy ordering.

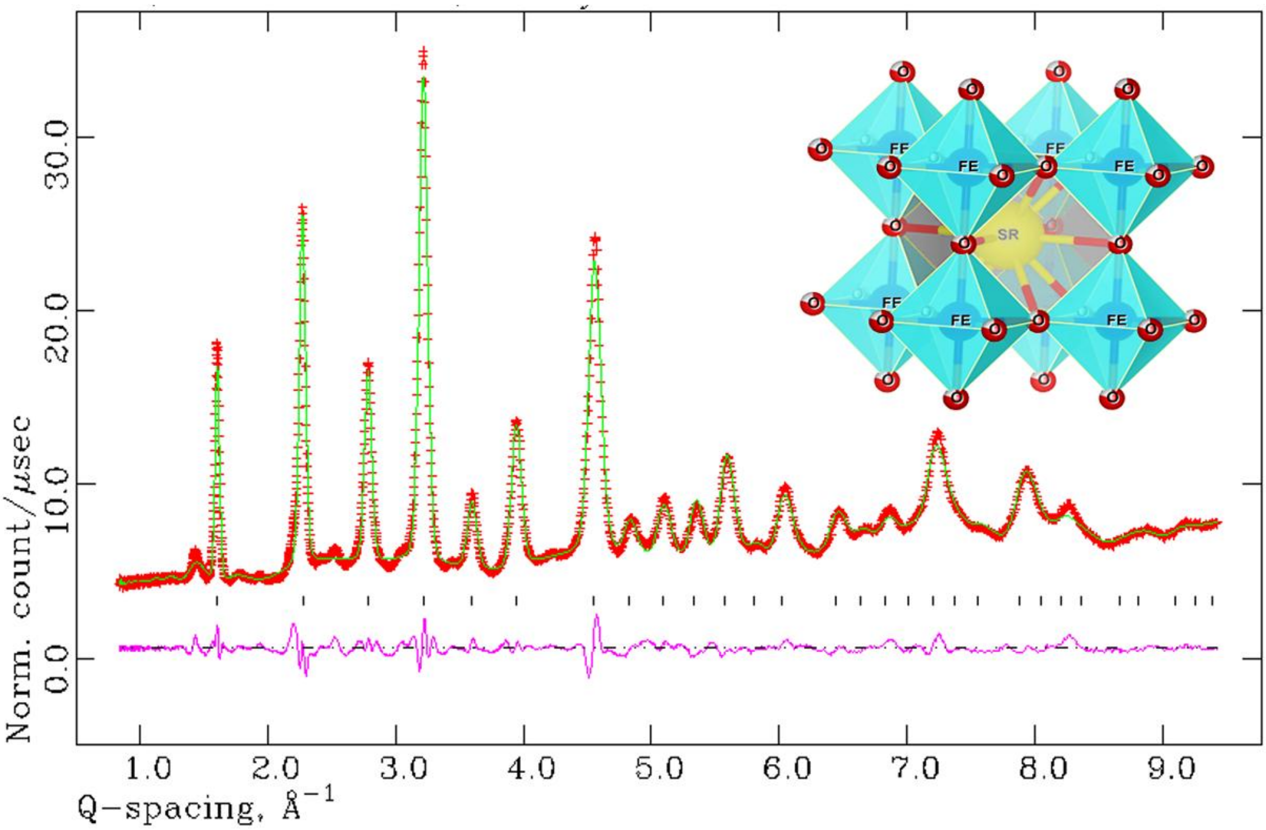

Figure 1. a) Rietveld refinement profile at room temperature for $SrFe_{0.6}Cu_{0.3}Mo_{0.1}O_{3-\delta}$.
The original data is represented by a crossline (red), the measured profile data is depicted by a continuous line (green), and the difference is shown by a bottom line (purple) with a 3D polyhedral representation of $SrFe_{0.6}Cu_{0.3}Mo_{0.1}O_{3-\delta}$ in it

Table 1

Rietveld refinement parameters for $SrFe_{0.6}Cu_{0.3}Mo_{0.1}O_{3-\delta}$ at room temperature (space group *Pm-3m*), atomic coordinates and isotropic temperature factors (U_{iso})

Parameters	$SrFe_{0.6}Cu_{0.3}Mo_{0.1}O_{3-\delta}$
Structure model	Cubic
Space group	*Pm-3m*
Volume (Å^3)	271.5090
R-factors	
R_f (%)	3.38
R_p (%)	2.94
R_{wp} (%)	4.36
Cell parameters	
a (Å)	3.8997 (1)
b (Å)	3.8997 (1)
c (Å)	3.8997 (1)
Atomic positions	*x*, *y*, *z*
Sr (1b)	0.5000, 0.5000, 0.0000
U_{iso} (Å^2)	0.0176 (1)
Fe (1a)	0.0000, 0.0000, 0.0000
U_{iso} (Å^2)	0.0045 (2)
Cu (1a)	0.0000, 0.0000, 0. 0.0000
U_{iso} (Å^2)	0.8000 (2)
Mo (1a)	0.0000, 0.0000, 0. 0.0000
U_{iso} (Å^2)	0.0183 (1)
O (3d)	0.5000, 0.0000, 0.0000
U_{iso} (Å^2)	0.0165 (1)

Bond Length Analysis

For an ideal cubic perovskite (ABO_3) structure, the bond lengths are given by $d_a - O = a/\sqrt{2}$ and $d_b - O = a/2$, where *a* is the lattice constant. The experimentally refined bond lengths for $SrFe_{0.6}Cu_{0.3}Mo_{0.1}O_{3-\delta}$ are listed in Table 2. The average B–O bond length was found to be 1.946 Å, in close agreement with the theoretical value calculated from the lattice constant and Shannon ionic radii [43].

Table 2

Bond distances for cubic $SrFe_{0.6}Cu_{0.3}Mo_{0.1}O_{3-\delta}$ in (Å) ($d \leq 6$ Å) extracted at room temperature (RT), based on NPD data

Bond	Multiplicity	Bond length (Å)
$Sr–O_1$	×12	2.75233 (3)
$Fe–O_1$	×6	1.94619 (3)
$Cu–O_1$	×6	1.94619 (3)
$Mo–O_1$	×6	1.94619 (3)

The absence of additional reflections in the NPD pattern suggests no symmetry reduction or long-range cation ordering, confirming that oxygen vacancies and cation substitutions do not induce structural distortion detectable within the resolution of the diffraction data.

The bond lengths obtained from the refinement were very close to the calculated bond lengths. The experimental bond length (B–O) for $SrFe_{0.6}Cu_{0.3}Mo_{0.1}O_{3-\delta}$ was obtained at 1.9462 Å (Table 2). The NPD layout measured at room temperature was appropriately refined in the space group *Pm*-3*m* and the polyhedral representation of the crystal structure as shown in Figure 1, displaying no extra peaks that ought to activist a superstructure bobbing up from oxygen vacancies or the long-range ordering of metals, or a reduction in symmetry.

Microstructural Characterization

The microstructure of the sample was examined using scanning electron microscopy (SEM) coupled with energy-dispersive X-ray spectroscopy (EDX). As shown in Figure 2, the SEM image reveals a porous and interconnected grain network, consistent with the open morphology typically observed in perovskite oxides synthesized via solid-state routes. The microstructure is composed of micrometer-sized agglomerates formed by the sintering of irregular nanocrystalline particles.

The presence of Cu^{2+} ions promotes enhanced grain growth and neck formation during sintering, leading to a partially fused morphology [44, 45]. The average grain size was approximately 1 μm, and EDX analysis confirmed a homogeneous elemental distribution of Sr, Fe, Cu, Mo, and O without detectable impurity phases. This uniformity further supports the single-phase nature of the compound as observed in the NPD and XRD analyses.

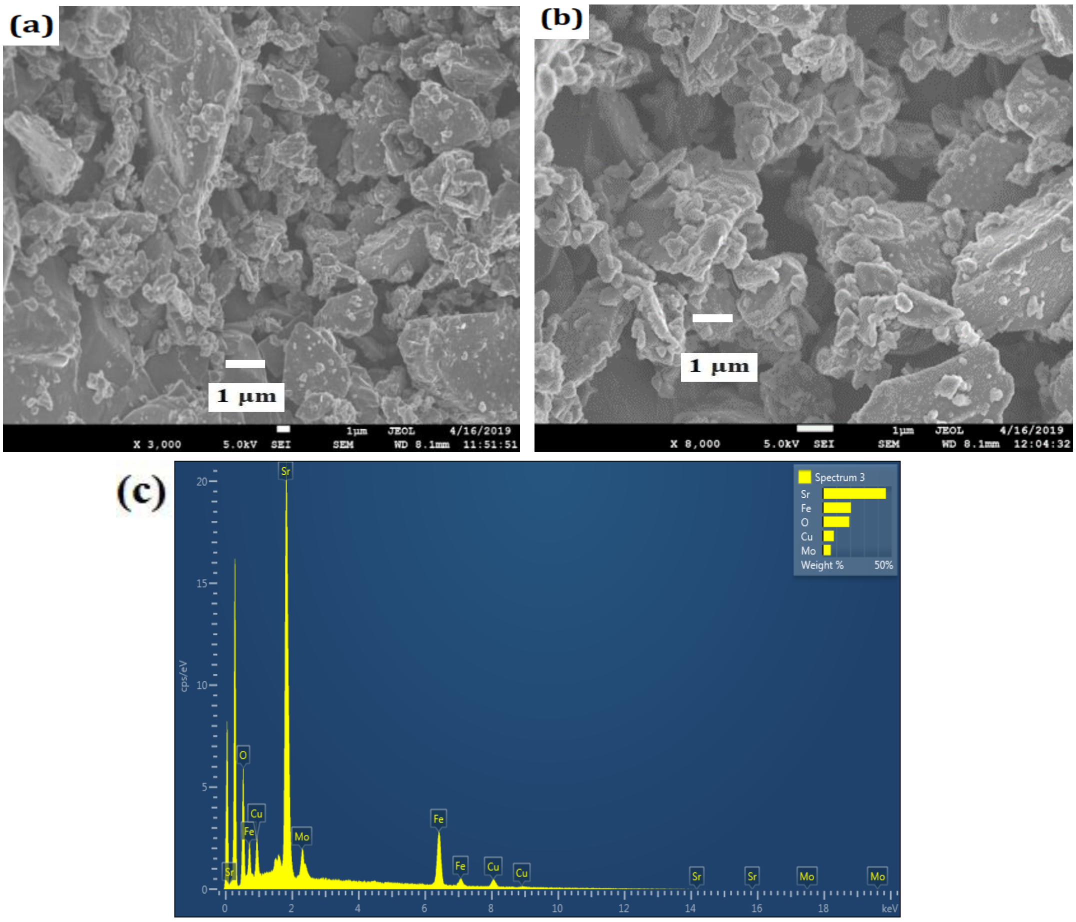

Figure 2. Scanning electron micrographs for $SrFe_{0.6}Cu_{0.3}Mo_{0.1}O_{3-\delta}$ pellet using a secondary electron image (SEI) detector with a low voltage (5.0 kV) with carbon-coated specimen and the associated EDS spectrum is shown in the inset

Thermal Analysis and Thermal Conductivity

Thermogravimetric analysis (TGA) of $SrFe_{0.6}Cu_{0.3}Mo_{0.1}O_{3-\delta}$ revealed a distinct two-stage weight loss pattern (Fig. 3). A sharp decrease in mass was observed up to 400 °C, similar to the thermal behavior reported by Rattiphorn et al. [44]. This initial weight loss is attributed to the release of physically adsorbed species and the partial oxidation of transition-metal cations. Between 400 °C and 650 °C, the weight loss proceeded gradually, corresponding to further oxidation reactions within the lattice and the formation of higher metal oxides. At elevated temperatures, CuO can partially decompose to Cu_2O, contributing to the observed mass change [45].

Copper-containing mixed oxides are widely recognized for their high oxygen exchange capacity and enhanced redox reactivity, which improve the performance of composite oxygen carriers and other functional materials [46–48]. To maintain an inert environment during the TGA experiment, the analysis was conducted under a nitrogen-rich atmosphere within a vacuum-sealed chamber. The onset of oxidation near 400 °C confirmed the sample's reactive oxygen mobility under thermal excitation.

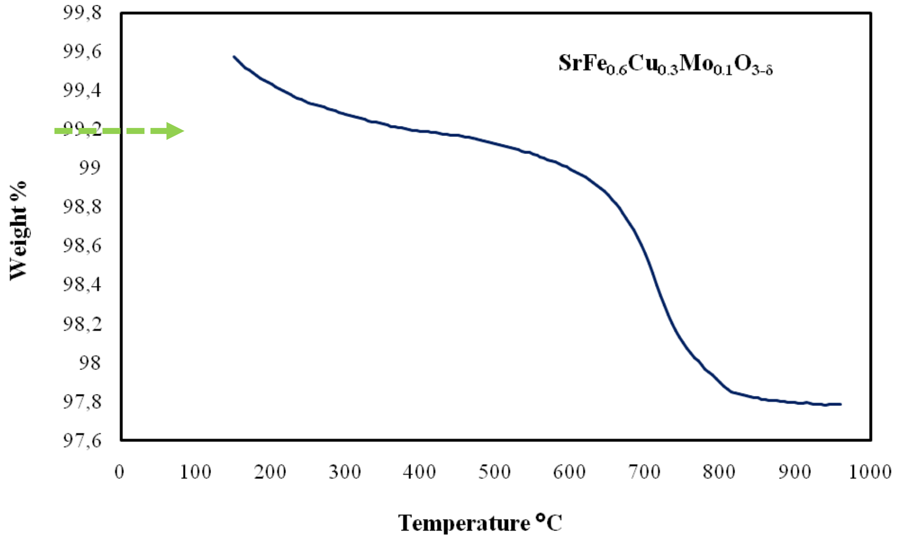

Figure 3. TGA diagram of $SrFe_{0.6}Cu_{0.3}Mo_{0.1}O_{3-\delta}$ on a scale of 20 °C to 950 °C

Differential scanning calorimetry (DSC) measurements (Fig. 4) further revealed a gradual increase in heat flow between room temperature and 110 °C, associated with the release of surface-bound volatiles. Two broad endothermic peaks appeared at 914 °C and 949 °C, followed by an endothermic transition near 104 °C, indicating structural rearrangements and oxygen loss at high temperature.

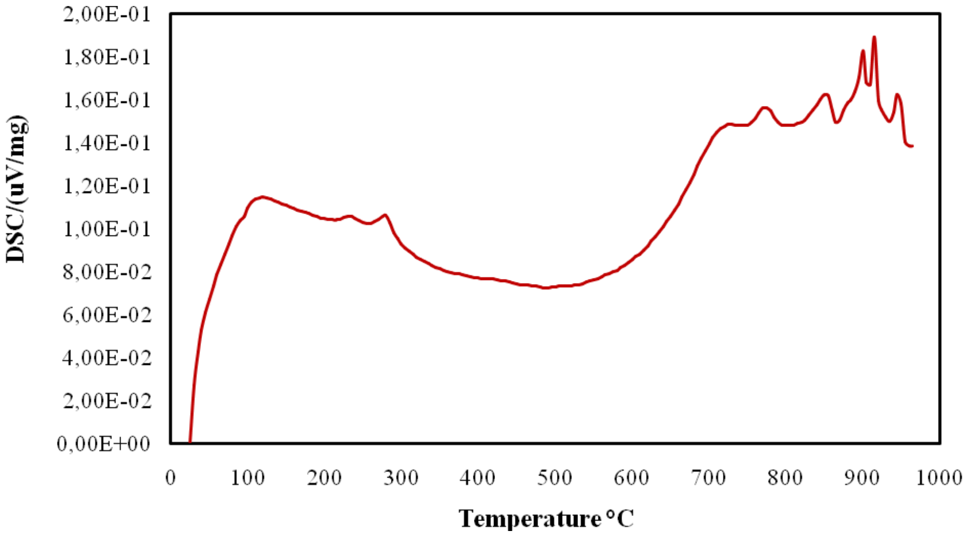

Figure 4. DSC diagram of $SrFe_{0.6}Cu_{0.3}Mo_{0.1}O_{3-\delta}$ on a scale of 25 °C to 950 °C

Thermal conduction in oxides primarily arises from phonon transport, governed by the mobility of lattice vibrations. Unlike metals, where free electrons dominate heat transfer, ceramic oxides exhibit inherently low thermal conductivity due to their predominantly ionic bonding and phonon scattering at grain boundaries. Additional microstructural factors such as porosity and grain interfaces further impede heat transport.

Perovskite-type oxides have, therefore, attracted considerable attention as low-thermal-conductivity materials with high structural stability at elevated temperatures [49, 50]. The measured thermal conductivity (κ) of $SrFe_{0.6}Cu_{0.3}Mo_{0.1}O_{3-\delta}$ from room temperature to 900 °C is presented in Figure 5. The oxide exhibited a value of 1.986 $Wm^{-1}K^{-1}$ at 900 °C, comparable to other complex perovskites such as $Sr_{0.9}La_{0.1}(Zr_{0.25}Sn_{0.25}Ti_{0.25}Hf_{0.25})O_3$ (1.89 $Wm^{-1}K^{-1}$ at 873 K) [51, 52] and significantly lower than undoped $SrTiO_3$ (10 W m^{-1} K^{-1} at 300 K) [53].

This reduction in κ can be attributed to enhanced phonon scattering caused by B-site cation disorder (Fe, Cu, Mo), oxygen vacancies, and the porous microstructure observed by SEM. These defects disrupt lattice periodicity and inhibit coherent phonon propagation. As summarized in Table 3, $SrFe_{0.6}Cu_{0.3}Mo_{0.1}O_{3-\delta}$ demonstrates one of the lowest thermal conductivities among single-phase cubic perovskites, confirming that Cu/Mo co-doping effectively tunes lattice dynamics without compromising phase stability.

Such a combination of structural stability, oxygen mobility, and low thermal conductivity suggests strong potential for this material in high-temperature thermoelectric and SOFC applications, where maintaining temperature gradients and minimizing heat loss are essential for improved performance and longevity.

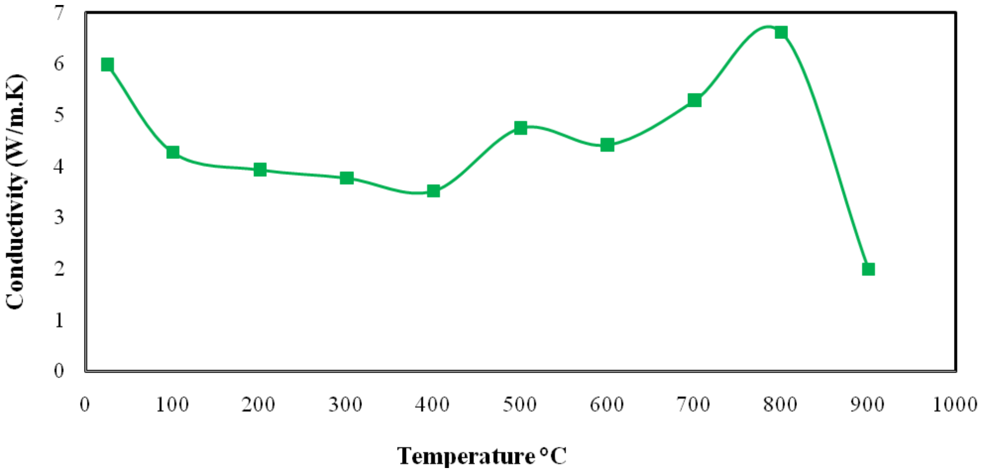

Figure 5. Thermal conductivity of $SrFe_{0.6}Cu_{0.3}Mo_{0.1}O_{3-\delta}$ on a scale of 25 °C to 900 °C

Table 3

Comparison of thermal conductivities for $SrFe_{0.6}Cu_{0.3}Mo_{0.1}O_{3-\delta}$ and other perovskite structures in the literature

Compositions	Temperature	Thermal conductivity ($Wm^{-1}K^{-1}$)	Ref.
$Sr_{0.9}La_{0.1}(Zr_{0.25}Sn_{0.25}Ti_{0.25}Hf_{0.25})O_3$	873 K	1.89	[52]
$(Ca_{0.25}Sr_{0.25}Ba_{0.25}La_{0.25})TiO_3$	1073 K	2.5	[54]
$SrZrO_3$	1273 K	2.1	[55]
$SrTiO_3$	300 K	10	[53]
$SrFe_{0.6}Cu_{0.3}Mo_{0.1}O_{3-\delta}$	1173 K	1.986	This work

Compared to other perovskites possessing single-phase cubic structures, $SrFe_{0.6}Cu_{0.3}Mo_{0.1}O_{3-\delta}$ exhibits a notably low thermal conductivity, as summarized in Table 3. The structural and thermal analyses indicate that the sample combines high porosity with good phase stability and a controlled degree of oxygen deficiency, which collectively contribute to its favorable thermal behavior. In this composition, the B-site cations (Fe, Cu, and Mo) occupy corner-shared octahedral sites within the cubic perovskite lattice, forming a well-defined and symmetrical framework.

The incorporation of Cu into the perovskite matrix not only promotes electronic conductivity but also modifies the lattice dynamics, enhancing phonon scattering and thereby reducing thermal transport. The resulting microstructure, characterized by a highly porous and interconnected network, facilitates effective charge mobility while impeding heat conduction. Thermogravimetric analysis revealed weight loss primarily between 200 °C and 950 °C, corresponding to oxygen release and the formation of thermally stable oxide phases.

Overall, the combination of single-phase cubic symmetry, controlled oxygen non-stoichiometry, and low thermal conductivity suggests that $SrFe_{0.6}Cu_{0.3}Mo_{0.1}O_{3-\delta}$ is a promising candidate for high-temperature thermoelectric and solid oxide fuel cell applications, where materials with low heat transport and stable structural integrity are essential.

Conclusion

A single-phase cubic perovskite oxide $SrFe_{0.6}Cu_{0.3}Mo_{0.1}O_{3-\delta}$ was successfully synthesized via the solid-state reaction method and characterized using neutron powder diffraction, scanning electron microscopy, and thermal analyses. Rietveld refinement of the neutron diffraction data confirmed that the material crystallizes in a simple cubic structure with space group *Pm*-3*m* and a lattice parameter of a = 3.8997(1) Å. The microstructural analysis revealed a homogeneous, porous morphology with interconnected grains, while TGA and DSC results demonstrated thermal stability up to 950 °C with oxygen release occurring in two main stages.

The measured thermal conductivity of 1.986 $Wm^{-1}K^{-1}$ at 900 °C indicates that Cu and Mo co-doping at the B-site effectively enhances phonon scattering and reduces heat transport without disrupting the structural integrity of the perovskite lattice. The combined characteristics of structural stability, controlled oxygen non-stoichiometry, and low thermal conductivity make $SrFe_{0.6}Cu_{0.3}Mo_{0.1}O_{3-\delta}$ a promising candidate for high-temperature energy applications such as solid oxide fuel cells and thermoelectric devices.

Future work will focus on correlating electrical conductivity and Seebeck coefficient data with the present thermal results to evaluate the overall thermoelectric performance and optimize the dopant concentration for enhanced functional efficiency.

Acknowledgment

This research was funded by the grant with reference number AP26103025, provided by the Ministry of Science and Higher Education of Kazakhstan. The authors are profoundly grateful to the L.N. Gumilyov Eurasian National University, Kazakhstan; Universiti Brunei Darussalam, Brunei; Chalmers University of Technology, Sweden for facilitating the work. The authors would also like to show gratitude to Professor Paul Henry and the ISIS Neutron and Muon facility in the UK for their scheduled beam-time.

References

1 Si, C., Zhang, W., Lu, Q., Guo, E., Yang, Z., Chen, J., He, X., & Luo, J. (2022). Recent advances in perovskite catalysts for efficient overall water splitting. *Catalysts, 12*(6), 601. https://doi.org/10.3390/catal12060601

2 Locock, A. J., & Mitchell, R.H. (2018). Perovskite classification: An Excel spreadsheet to determine and depict end-member proportions for the perovskite- and vapnikite-subgroups of the perovskite supergroup. *Computers & Geosciences, 113*, 106–114. https://doi.org/10.1016/j.cageo.2018.01.012

3 Jiang, W., Luo, W., Wang, J., Zhang, M., & Zhu, Y. (2016). Enhancement of catalytic activity and oxidative ability for graphitic carbon nitride. *Journal of Photochemistry and Photobiology C: Photochemistry Reviews, 28*, 87–115. https://doi.org/10.1016/j.jphotochemrev.2016.06.001

4 Mirzaei, M., Zarch, M.B., Darroudi, M., Sayyadi, K., Keshavarz, S.T., Sayyadi, J., Fallah, A., & Maleki, H. (2020). Silica mesoporous structures: Effective nanocarriers in drug delivery and nanocatalysts. *Applied Sciences, 10*(21), 7533. https://doi.org/10.3390/app10217533

5 Lu, Y., Zhang, Z., Wang, H., & Wang, Y. (2021). Toward efficient single-atom catalysts for renewable fuels and chemicals production from biomass and CO_2. *Applied Catalysis B: Environmental, 292*, 120–162. https://doi.org/10.1016/j.apcatb.2021.120162

6 Wang, R.T., Chang, H.Y., & Wang, J.C. (2021). An overview on the novel core–shell electrodes for solid oxide fuel cell (SOFC) using polymeric methodology. *Polymers, 13*(16), 2774. https://doi.org/10.3390/polym13162774

7 Madhavan, B., Suvitha, A., Steephen, A., & Pillai, M.B. (2022). Novel $La_{1-x}Ca_xTi_{1-\gamma}Ta_\gamma O_{3-\delta}$ perovskites with enhanced conductivity for solid oxide fuel cell electrodes. *Journal of Alloys and Compounds, 915*, 165370. https://doi.org/10.1016/j.jallcom.2022.165370

8 Cai, H., Xu, J., Wu, M., Long, W., Zhang, L., Song, Z., & Zhang, L. (2020). A novel cobalt-free $La_{0.5}Ba_{0.5}Fe_{0.95}Mo_{0.05}O_{3-\delta}$ electrode for symmetric solid oxide fuel cell. *Journal of the European Ceramic Society, 40*(12), 4361–4365. https://doi.org/10.1016/j.jeurceramsoc.2020.04.050

9 Song, J., Zhu, T., Chen, X., Ni, W., & Zhong, Q. (2020). Cobalt and titanium substituted $SrFeO_3$-based perovskite as efficient symmetrical electrode for solid oxide fuel cell. *Journal of Materials, 6*(2), 377–384. https://doi.org/10.1016/j.jmat.2020.02.009

10 Li, Q., Xia, T., Sun, L., Zhao, H., & Huo, L. (2014). Electrochemical performance of novel cobalt-free perovskite $SrFe_{0.7}Cu_{0.3}O_{3-\delta}$ cathode for intermediate temperature solid oxide fuel cells. *Electrochimica Acta, 150*, 151–156. https://doi.org/10.1016/j.electacta.2014.10.137

11 Ksepko, E. (2018). Perovskite $Sr(Fe_{1-x}Cu_x)O_{3-\delta}$ materials for chemical looping combustion applications. *International Journal of Hydrogen Energy, 43*(20), 9622–9634. https://doi.org/10.1016/j.ijhydene.2018.04.046

12 Omeiza, L.A., Kabyshev, A., Bekmyrza, K., Kubenova, M., Kuterbekov, K. A., Baratova, A., Adaikhan, S., Bakar, S.A., & Azad, A.K. (2024). Strontium-doped $BaZr_{0.8}Ni_{0.2}O_{3-\delta}$ cobalt-free cathode materials for solid oxide fuel cell. *International Journal of Precision Engineering and Manufacturing — Green Technology, 12*, 1295–1307. https://doi.org/10.1007/s40684-024-00667-z

13 Omeiza, L.A., Rahman, M.M., Kuterbekov, K.A., Kabyshev, A., Bekmyrza, K., Kubenova, M., Somalu, M.R., Bakar, S.A., & Azad, A.K. (2024). Novel Sr-doped $NdMn_{0.5}Cr_{0.5}O_{3-\delta}$ electrodes for symmetrical solid oxide fuel cell. *Electrochemistry Communications, 164*, 107730. https://doi.org/10.1016/j.elecom.2024.107730

14 Omeiza, L.A., Kuterbekov, K.A., Kabyshev, A., Bekmyrza, K., Kubenova, M., Afroze, S., Bakar, S.A., & Azad, A.K. (2024). Limitations and trends on cobalt-free cathode materials development for intermediate-temperature solid oxide fuel cell: An updated technical review. *Emergent Materials, 7*, 2189–2204. https://doi.org/10.1007/s42247-024-00737-7

15 Omeiza, L.A., Kabyshev, A., Bekmyrza, K., Kuterbekov, K.A., Kubenova, M., Zhumadilova, Z.A., Subramanian, Y., Ali, M., Aidarbekov, N., & Azad, A.K. (2025). Constraints in sustainable electrode materials development for solid oxide fuel cell: A brief review. *Materials Science for Energy Technologies, 8*, 32–43. https://doi.org/10.1016/j.mset.2024.07.001

16 Kuterbekov, K.A., Bekmyrza, K.Zh., Kabyshev, A.M., Kubenova, M.M., Aidarbekov, N.K., & Nurkenov, S.A. (2022). Investigation of the Characteristics of Materials with the Ruddlesden-Popper Structure for Solid Oxide Fuel Cells. *Bulletin of the University of Karaganda-Physics*, *4*(108), 32–47. https://doi.org/10.31489/2022ph4/32-47

17 Adaikhan, S., Bekmyrza, K.Zh., Baratova, A.A., Kabyshev, A.M., Rajagopal, P., Aidarbekov, N.K., Kuterbekov, K.K., Kubenova, M.M., & Kuanysh, M.D. (2025). Development and characterization of nanostructured Ni–ScSZ composite anodes for solid oxide fuel cells. *Bulletin of the University of Karaganda-Physics*, *3*(119), 16–30. https://doi.org/10.31489/2025ph3/16-30

18 Bakalbayeva, G.A., Baratova, A.A., Aidarbekov, N.K., Kubenova, M.M., Amangozhayeva, A.N., & Bisseken, R.S. (2025). Investigation of the functional characteristics of $Pr_{1-x}Sr_xFe_{1-\gamma}Co_\gamma O_{3-\delta}$ perovskite cathodes for reversible solid oxide fuel cells. *Bulletin of the University of Karaganda-Physics*, *4*(120), 16–25. https://doi.org/10.31489/2025ph4/16-25

19 Tao, S., & Irvine, J.T.S. (2006). Phase transition in perovskite oxide $La_{0.75}Sr_{0.25}Cr_{0.5}Mn_{0.5}O_{3-\delta}$ observed by in situ high-temperature neutron powder diffraction. *Chemistry of Materials, 18*(23), 5453–5460. https://doi.org/10.1021/cm061413n

20 Afroze, S., Torino, N., Henry, P.F., Reza, M.S., Cheok, Q., & Azad, A.K. (2020). Insight of novel layered perovskite $PrSrMn_2O_{5+\delta}$: A neutron powder diffraction study. *Materials Letters, 261*, 127126. https://doi.org/10.1016/j.matlet.2019.127126

21 Hesse, F., Da Silva, I., & Bos, J.W.G. (2022). Insights into oxygen migration in $LaBaCo_2O_{6-\delta}$ perovskites from in situ neutron powder diffraction and bond valence site energy calculations. *Chemistry of Materials, 34*(3), 1191–1202. https://doi.org/10.1021/acs.chemmater.1c03726

22 Basbus, J.F., Arce, M.D., Napolitano, F.R., Troiani, H.E., Alonso, J.A., Saleta, M.E., González, M.A., Cuello, G.J., Fernández-Díaz, M.T., Sainz, M.P., Bonanos, N., Jimenez, C.E., Giebeler, L., Figueroa, S.J.A., Caneiro, A., Serquis, A.C., & Mogni, L.V. (2020). Revisiting the crystal structure of $BaCe_{0.4}Zr_{0.4}Y_{0.2}O_{3-\delta}$ proton conducting perovskite and its correlation with transport properties. *ACS Applied Energy Materials, 3*(3), 2881–2892. https://doi.org/10.1021/acsaem.9b02498

23 Basbus, J.F., Arce, M.D., Alonso, J.A., González, M.A., Cuello, G.J., Fernández-Díaz, M.T., Sha, Z., Skinner, S.J., Mogni, L.V., & Serquis, A.C. (2022). In situ neutron diffraction study of $BaCe_{0.4}Zr_{0.4}Y_{0.2}O_{3-\delta}$ proton conducting perovskite: Insight into the phase transition and proton transport mechanism. *Journal of Materials Chemistry A, 10*(17), 9037–9047. https://doi.org/10.1039/d1ta10789e

24 Moos, R., Bischoff, T., Menesklou, W., & Härdtl, K.H. (1997). Solubility of lanthanum in strontium titanate in oxygen-rich atmospheres. *Journal of Materials Science*, *32*, 4247–4252. https://doi.org/10.1023/A:1018647117607

25 Lu, Z., Zhang, H., Lei, W., Sinclair, D.C., & Reaney, I.M. (2016). High-figure-of-merit thermoelectric La-doped A-site-deficient $SrTiO_3$ ceramics. *Chemistry of Materials, 28*(3), 925–935. https://doi.org/10.1021/acs.chemmater.5b04616

26 Han, J., Sun, Q., & Song, Y. (2017). Enhanced thermoelectric properties of La- and Dy-co-doped, Sr-deficient $SrTiO_3$ ceramics. *Journal of Alloys and Compounds, 705*, 22–27. https://doi.org/10.1016/j.jallcom.2017.02.146

27 Kovalevsky, A.V., Yaremchenko, A.A., Populoh, S., Thiel, P., Fagg, D.P., Weidenkaff, A., & Frade, J.R. (2014). Towards a high thermoelectric performance in rare-earth substituted $SrTiO_3$: Effects provided by strongly reducing sintering conditions. *Physical Chemistry Chemical Physics, 16*, 26946–26954. https://doi.org/10.1039/c4cp04127e

28 Gong, J., Yuan, Z., Xu, S., Li, Z., Xu, J., & Tang, G. (2017). Investigation of the thermoelectric properties of Nb- and oxygen-vacancy-co-doped $SrTiO_3$ ceramics. *Materials Research Express, 4*, 055504. https://doi.org/10.1088/2053-1591/aa6d04

29 Ohta, S., Ohta, H., & Koumoto, K. (2006). Grain size dependence of thermoelectric performance of Nb-doped $SrTiO_3$ polycrystals. *Journal of the Ceramic Society of Japan*, *114*(1325), 102–105. https://doi.org/10.2109/jcersj.114.102

30 Leventouri, T., Bunaciu, C.E., & Perdikatsis, V. (2003). Neutron powder diffraction studies of silicon-substituted hydroxyapatite. *Biomaterials*, *24*(23), 4205–4211. https://doi.org/10.1016/S0142-9612(03)00333-8

31 Jiang, S.P., Zhang, L., He, H.Q., Yap, R.K., & Xiang, Y. (2009). Synthesis and characterization of lanthanum silicate apatite by gel-casting route as electrolytes for solid oxide fuel cells. *Journal of Power Sources, 189*(2), 972–981. https://doi.org/10.1016/j.jpowsour.2008.12.064

32 Karim, A.H., Park, K.-Y., Lee, T.H., Ali, S.A.M., Hossain, S., Absah, H.Q.H.H., Park, J.-Y., & Azad, A.K. (2017). Synthesis, structure and electrochemical performance of double perovskite oxide $Sr_2Fe_{1-x}Ti_xNbO_{6-\delta}$ as SOFC electrode. *Journal of Alloys and Compounds, 724*, 666–673. https://doi.org/10.1016/j.jallcom.2017.07.059

33 Azad, A.K., Ivanov, S.A., Eriksson, S.-G., Eriksen, J., Rundlöf, H., Mathieu, R., & Svedlindh, P. (2001). Synthesis, crystal structure, and magnetic characterization of the double perovskite Ba_2MnWO_6. *Materials Research Bulletin, 36*(12), 2215–2228. https://doi.org/10.1016/S0025-5408(01)00707-3

34 Afroze, S., Torino, N., Henry, P.F., Reza, M.S., Cheok, Q., & Azad, A.K. (2020). Neutron and X-ray powder diffraction data to determine the structural properties of novel layered perovskite $PrSrMn_2O_{5+\delta}$. *Data in Brief, 29*, 105173. https://doi.org/10.1016/j.dib.2020.105173

35 Rahman, S.M.H., Norberg, S.T., Knee, C.S., Biendicho, J.J., Hull, S., & Eriksson, S.G. (2014). Proton conductivity of hexagonal and cubic $BaTi_{1-x}Sc_xO_{3-\Delta}$ $(0.1 \le x \le 0.8)$. *Dalton Transactions*, *43*, 15055–15064. https://doi.org/10.1039/c4dt01280a

36 Smith, R.I., Hull, S., Tucker, M.G., Playford, H.Y., McPhail, D.J., Waller, S.P., & Norberg, S.T. (2019). The upgraded Polaris powder diffractometer at the ISIS neutron source. *Review of Scientific Instruments, 90*, 115101–115113. https://doi.org/10.1063/1.5099568

37 Hull, S., Smith, R.I., David, W.I.F., Hannon, A.C., Mayers, J., & Cywinski, R. (1992). The Polaris powder diffractometer at ISIS. *Physica B: Condensed Matter, 180-181*, 1000–1002. https://doi.org/10.1016/0921-4526(92)90533-X

38 Toby, B.H., & Von Dreele, R.B. (2013). GSAS-II: The genesis of a modern open-source all-purpose crystallography software package. *Journal of Applied Crystallography, 46*, 544–549. https://doi.org/10.1107/S0021889813003531

39 Cowin, P.I., Lan, R., Petit, C.T.G., Du, D., Xie, K., Wang, H., & Tao, S. (2017). Conductivity and redox stability of new perovskite oxides $SrFe_{0.7}TM_{0.2}Ti_{0.1}O_{3-\delta}$ (TM = Mn, Fe, Co, Ni, Cu). *Solid State Ionics, 301*, 99–105. https://doi.org/10.1016/j.ssi.2017.01.017

40 Cowin, P.I., Lan, R., Petit, C.T.G., & Tao, S. (2015). Conductivity and redox stability of perovskite oxide $SrFe_{1-x}Ti_xO_{3-\delta}$ ($x \le 0.3$). *Solid State Sciences, 46*, 62–70. https://doi.org/10.1016/j.solidstatesciences.2015.05.004

41 Cho, S., Fowler, D.E., Miller, E.C., Cronin, J.S., Poeppelmeier, K.R., & Barnett, S.A. (2013). Fe-substituted $SrTiO_{3-\delta}Ce_{0.9}Gd_{0.1}O_2$ composite anodes for solid oxide fuel cells. *Energy & Environmental Science, 6*, 1850–1857. https://doi.org/10.1039/c3ee23791e

42 Lan, R., Cowin, P.I., Sengodan, S., & Tao, S. (2016). A perovskite oxide with high conductivities in both air and reducing atmosphere for use as electrode for solid oxide fuel cells. *Scientific Reports, 6*, 31839. https://doi.org/10.1038/srep31839

43 Shannon, R.D. (1976). Revised effective ionic radii and systematic studies of interatomic distances in halides and chalcogenides. *Acta Crystallographica Section A, 32*, 751–767. https://doi.org/10.1107/S0567739476001551

44 Sumang, R., & Bongkarn, T. (2011). The influences of firing temperatures and excess PbO on the crystal structure and microstructure of $(Pb_{0.25}Sr_{0.75})TiO_3$ ceramics. *Journal of Materials Science, 46*, 6823–6829. https://doi.org/10.1007/s10853-011-5641-2

45 Barbooti, M.M. (1984). Thermal behaviour of copper oxides and copper sulphate in the presence of carbon. *Solar Energy Materials, 10*(1), 35–40. https://doi.org/10.1016/0165-1633(84)90005-4

46 Yang, W., Zhao, H., Wang, K., & Zheng, C. (2015). Synergistic effects of mixtures of iron ores and copper ores as oxygen carriers in chemical-looping combustion. *Proceedings of the Combustion Institute, 35*(3), 2811–2818. https://doi.org/10.1016/j.proci.2014.07.010

47 Siriwardane, R., Benincosa, W., Riley, J., Tian, H., & Richards, G. (2016). Investigation of reactions in a fluidized bed reactor during chemical looping combustion of coal/steam with copper oxide–iron oxide–alumina oxygen carrier. *Applied Energy, 183*, 1550–1564. https://doi.org/10.1016/j.apenergy.2016.09.045

48 Duan, L., Godino, D., Manovic, V., Montagnaro, F., & Anthony, E.J. (2016). Cyclic oxygen release characteristics of bifunctional copper oxide/calcium oxide composites. *Energy Technology, 4*(10), 1171–1178. https://doi.org/10.1002/ente.201600028

49 Liu, Y., Jia, D., Zhou, Y., Zhou, Y., Zhao, J., Nian, H., & Liu, B. (2020). $Zn_{0.1}Ca_{0.1}Sr_{0.4}Ba_{0.4}ZrO_3$: A non-equimolar multi-component perovskite ceramic with low thermal conductivity. *Journal of the European Ceramic Society, 40*(15), 6272–6277. https://doi.org/10.1016/j.jeurceramsoc.2020.07.054

50 Zhao, Z., Xiang, H., Dai, F.Z., Peng, Z., & Zhou, Y. (2019). $(La_{0.2}Ce_{0.2}Nd_{0.2}Sm_{0.2}Eu_{0.2})_2Zr_2O_7$: A novel high-entropy ceramic with low thermal conductivity and sluggish grain growth rate. *Journal of Materials Science & Technology, 35*(11), 2647–2651. https://doi.org/10.1016/j.jmst.2019.05.054

51 Banerjee, R., Chatterjee, S., Ranjan, M., Bhattacharya, T., Mukherjee, S., Jana, S.S., Dwivedi, A., & Maiti, T. (2020). High-Entropy Perovskites: An Emergent Class of Oxide Thermoelectrics with Ultralow Thermal Conductivity. *ACS Sustainable Chemistry & Engineering, 8*(46), 17022–17032. https://doi.org/10.1021/acssuschemeng.0c03849

52 Lou, Z., Zhang, P., Zhu, J., Gong, L., Xu, J., Chen, Q., Reece, M.J., Yan, H., & Gao, F. (2022). A novel high-entropy perovskite ceramic $Sr_{0.9}La_{0.1}(Zr_{0.25}Sn_{0.25}Ti_{0.25}Hf_{0.25})O_3$ with low thermal conductivity and high Seebeck coefficient. *Journal of the European Ceramic Society, 42*(8), 3480–3488. https://doi.org/10.1016/j.jeurceramsoc.2022.02.053

53 Ekren, D., Azough, F., & Freer, R. (2019). Enhancing the thermoelectric properties of $Sr_{1-x}Pr_{2x/3\pm x/3}TiO_{3\pm\delta}$ through control of crystal structure and microstructure. *Philosophical Transactions of the Royal Society A: Mathematical, Physical and Engineering Sciences, 377*, 20190037. https://doi.org/10.1098/rsta.2019.0037

54 Zhang, P., Gong, L., Lou, Z., Xu, J., Cao, S., Zhu, J., Yan, H., & Gao, F. (2022). Reduced lattice thermal conductivity of perovskite-type high-entropy $(Ca_{0.25}Sr_{0.25}Ba_{0.25}Re_{0.25})TiO_3$ ceramics by phonon engineering for thermoelectric applications. *Journal of Alloys and Compounds, 898*, 162858. https://doi.org/10.1016/j.jallcom.2021.162858

55 Ma, W., Jarligo, M.O., Mack, D.E., Pitzer, D., Malzbender, J., Va'en, R., & Stöver, D. (2008). New generation perovskite thermal barrier coating materials. *Journal of Thermal Spray Technology, 17*, 831–837. https://doi.org/10.1007/s11666-008-9239-4

Ш. Афрозе, А.М. Кабышев, А.А. Аймаханова,
М.С. Реза, М.С. Ислам, К.А. Кутербеков, А.К. Азад

Жаңа легирленген перовскит түріндегі $SrFe_{0.6}Cu_{0.3}Mo_{0.1}O_{3-\delta}$ оксидінің құрылымдық және жылулық қасиеттерін зерттеу

Жұмыста жаңа перовскит түріндегі $SrFe_{0.6}Cu_{0.3}Mo_{0.1}O_{3-\delta}$ оксиді қаттыфазалық реакция әдісімен синтезделіп, нейтрондық ұнтақ дифракциясы (НҰД), сканерлеуші электрондық микроскопия (СЭМ) және жылулық талдау әдістері арқылы жан-жақты сипатталды. НҰД қолдану атомдық құрылымды дәл анықтауға және атомдық нөмірлері ұқсас катиондарды ажыратуға мүмкіндік берді. Ритвельд әдісі бойынша алынған нәтижелер *Pm*-3*m* (№ 221) кеңістік тобына жататын кубтық бірфазалы перовскит құрылымының қалыптасуын растады, ал тор параметрі $a = b = c = 3.8997(1)$ Å болды. СЭМ кескіндері біртекті элементтік таралуы бар жоғары кеуекті және өзара байланысқан микроқұрылымды көрсетті. Термогравиметриялық талдау (ТГА) 1000 °С дейін екі сатылы оттегі жоғалтуды көрсетті, бұл материалдың жоғары жылулық тұрақтылығын дәлелдейді. 900 °С температурасында өлшенген жылуөткізгіштік 1.986 Вт·м$^{-1}$·К$^{-1}$ шамасында болып, Cu және Mo бірлесіп легирлеу нәтижесінде фонондардың шашырауының артуымен және тордың бұзылуымен түсіндіріледі. Алынған нәтижелер B-позициясындағы бақыланатын легирлеу дефекттік химияны және жылу тасымалын тиімді реттейтінін көрсетті. $SrFe_{0.6}Cu_{0.3}Mo_{0.1}O_{3-\delta}$ жоғары температуралы энергия түрлендіргіштерінде, соның ішінде термоэлектрлік құрылғылар мен қаттыоксидті отын элементтерінде қолдануға перспективті материал болып табылады.

Кілт сөздер: перовскит типті оксид, нейтрондық ұнтақ дифракциясы, Ритвельд әдісі, қаттыфазалық синтез, сканерлеуші электрондық микроскопия, термогравиметриялық талдау, микроструктура, оттегінің қаттылығы, фонондардың шашырауы, жылуөткізгіштік

Ш. Афрозе, А.М. Кабышев, А.А. Аймаханова,
М.С. Реза, М.С. Ислам, К.А. Кутербеков, А.К. Азад

Исследование структурных и тепловых свойств нового легированного оксида перовскитного типа $SrFe_{0.6}Cu_{0.3}Mo_{0.1}O_{3-\delta}$

В данной работе оксид $SrFe_{0.6}Cu_{0.3}Mo_{0.1}O_{3-\delta}$ был синтезирован методом твёрдофазной реакции и охарактеризован с использованием нейтронной порошковой дифракции (НПД), сканирующей электронной микроскопии (СЭМ) и термического анализа. Нейтронная дифракция позволяет проводить детальный анализ сложных оксидов, особенно в случаях, когда атомы имеют близкие атомные номера. Уточнение по методу Ритвельда данных НПД подтвердило простую кубическую перовскитную структуру с пространственной группой *Pm*-3*m* (№ 221) и параметрами элементарной ячейки $a = b = c = 3.8997(1)$ Å. Результаты СЭМ показали высокопористую и взаимосвязанную микроструктуру, в то время как термогравиметрический анализ (ТГА) выявил двухступенчатую потерю кислорода до 1000 °С, что указывает на хорошую термическую стабильность материала. Измеренная теплопроводность составила 1.986 Вт·м$^{-1}$·К$^{-1}$ при 900 °С. Полученные результаты демонстрируют, что содопирование медью и молибденом эффективно регулирует дефекты кристаллической решётки и рассеяние фононов, что открывает перспективные возможности для разработки перовскитных оксидов с пониженной теплопроводностью для применения в области альтернативной энергетики, их высокой термомеханической совместимости, улучшенной проводимости и долговечности.

Ключевые слова: оксид перовскитного типа, нейтронная порошковая дифракция, метод Ритвельда, твёрдофазный синтез, сканирующая электронная микроскопия, термогравиметрический анализ, микроструктура, нестрогость по кислороду, рассеяние фононов, теплопроводность

Information about the authors

Shammya, Afroze — Researcher of the Institute of Physical and Technical Sciences, L.N. Gumilyov Eurasian National University, Astana, Kazakhstan; Researcher of the Faculty of Integrated Technologies, Universiti Brunei Darussalam, Bandar Seri Begawan, Brunei; Researcher of the Department of Chemistry and Chemical Engineering, Chalmers University of Technology, Gothenburg, Sweden; e-mail: shammya111@gmail.com; Scopus ID: 57208761031; ORCID: https://orcid.org/0000-0002-8609-6001;

Kabyshev, Asset (*corresponding author*) — Teacher-Researcher of the Institute of Physical and Technical Sciences, L.N. Gumilyov Eurasian National University, Astana, Kazakhstan; e-mail: kabyshev_am_1@enu.kz; Scopus ID: 56177620700; ORCID: https://orcid.org/0000-0003-1472-4045

Aimakhanova, Ainur — PhD student of the Institute of Physical and Technical Sciences, L.N. Gumilyov Eurasian National University, Astana, Kazakhstan; e-mail: aimakhanova_aa@enu.kz.

MdSumon, Reza — Researcher of the Faculty of Integrated Technologies, University Brunei Darussalam, Bandar Seri Begawan, Brunei; e-mail: sumonce@gmail.com; Scopus ID: 57208498300; ORCID: https://orcid.org/0000-0002-7451-8385;

MdSirajul, Islam — Researcher of the Department of Civil Engineering, Bangladesh University of Engineering and Technology, Dhaka, Bangladesh; e-mail: mislam32@ncsu.eduж; ORCID: https://orcid.org/0009-0006-5365-6718

Kuterbekov, Kairat — Teacher-Researcher of the Institute of Physical and Technical Sciences, L.N. Gumilyov Eurasian National University, Astana, Kazakhstan; e-mail: kuterbekov_ka@enu.kz; Scopus ID: 6603440057; ORCID ID: https://orcid.org/0000-0001-5421-271X

Abul, K. Azad — Professor, Faculty of Integrated Technologies, University Brunei Darussalam, Bandar Seri Begawan, Brunei; Scopus ID: 56962736700; https://orcid.org/0000-0001-9391-3463; e-mail: abul.azad@ubd.edu.bn.